The contribution of mountains to global denudation

Isaac J. Larsen*, David R. Montgomery, and Harvey M. Greenberg
Department of Earth and Space Sciences and Quaternary Research Center, University of Washington, Seattle, Washington 98195, USA

ABSTRACT

The hypothesis that mountains influence global climate through links among rock uplift, physical and chemical denudation, and the carbon cycle remains vigorously debated. We address the contribution of mountains to global denudation with an empirical model that predicts that >50% of the total denudation and 40% of the chemical denudation occur on the steepest ~10% of Earth's terrestrial surface. These findings contrast with those from a recent study that suggested global-scale denudation occurs primarily on gently sloping terrain, but did not account for the influence of digital elevation model resolution on modeled denudation rates. Comparison of calculated denudation rates against the sum of measured sediment and solute yields from 265 watersheds indicates a positive correlation (R^2 = 0.44) with order-of-magnitude variability reflecting, among other things, the effects of dams and agriculture. In addition, ratios of measured river yield to modeled denudation rate decline as catchment area increases due to progressively greater sediment storage with increasing drainage area. Our results support the conclusion that the small mountainous fraction of Earth's surface dominates global denudation and the flux of sediment and solutes to oceans.

INTRODUCTION

Understanding the factors that influence the flux of dissolved and particulate material from land to oceans has key implications across the earth sciences, from global biogeochemical cycling, linking the sedimentary record with landscape dynamics, and environmental management. Knowledge of the controls on physical and chemical denudation rates is particularly relevant for evaluating Chamberlin's (1899) hypothesis that chemical denudation associated with mountain uplift drives global climate on geological time scales. The key links in this "uplift-climate" hypothesis are that tectonically driven surface uplift generates steep mountain topography, leading to rapid physical and chemical denudation. Chemical denudation of silicate minerals by carbonic acid releases Ca, Mg, and bicarbonate, which are delivered to oceans where they react to form carbonate minerals (Berner, 1991). Burial of carbonate rock, and organic carbon eroded from the terrestrial biosphere (France-Lanord and Derry, 1997), sequesters CO_2 from the ocean-atmosphere system, cooling global climate (Raymo et al., 1988).

Renewed interest in Chamberlin's (1899) uplift-climate hypothesis has produced ongoing debate over the role mountains play in regulating the carbon cycle (Molnar and England, 1990; Raymo and Ruddiman, 1992; Bickle, 1996; Berner and Caldeira, 1997; Willenbring and von Blanckenburg, 2010, among many others). Mountains are sites of high physical (Montgomery and Brandon, 2002) and chemical denudation rates (West et al., 2005). Chemical and physical denudation are correlated (e.g., Larsen et al., 2014), silicate cation denudation rates are coupled with chemical denudation rates (e.g., Gaillardet et al., 1999; West et al., 2005) (Fig. 1), and the transport of non-fossil organic carbon, which sequesters CO_2 if buried, is coupled with sediment yields in mountain rivers (e.g., Hilton et al., 2012). However, the proportion of Earth's surface with mountainous topography is small relative to more gently sloping lowlands, so understanding the role mountains play in present-day global denudation and weathering can yield insight into whether the uplift of mountains in the geological past may have perturbed global biogeochemical cycling.

Catchment-scale denudation rates (the sum of physical and chemical denudation rates) can be determined by measuring the concentration of ^{10}Be in sediment (e.g., Bierman and Steig, 1996). Such denudation rates integrate mass loss over 10^2 to 10^5 yr time scales and are insensitive to recent human-caused increases in denudation (von Blanckenburg, 2005). Multivariate analyses of a worldwide ^{10}Be data compilation indicate that catchment topography (slope and relief) is the dominant predictor of denudation rates, whereas other factors, including climate, explain little of the variability in catchment denudation rates (Portenga and Bierman, 2011).

Sediment and solute yields determined from river gauging and sediment monitoring data average over decadal time scales (e.g., Milliman and Farnsworth, 2011). Thus, anthropogenically driven erosion, pollution, dam construction, and low-frequency, high-magnitude events introduce substantial and systematic differences between measured sediment yields and long-term geologic averages (Milliman and Syvitski, 1992; Syvitski et al., 2005; Kirchner et al., 2001). As for denudation rates, catchment topography is the dominant influence on sediment yields, and climate plays a secondary role (Milliman and Syvitski, 1992; Summerfield and Hulton, 1994). Global delivery of sediment to oceans has been estimated to be ~19–20 Gt yr^{-1} (Milliman and Syvitski, 1992; Milliman and Farnsworth, 2011), but this value may be higher by a factor of 2 than yields prior to widespread

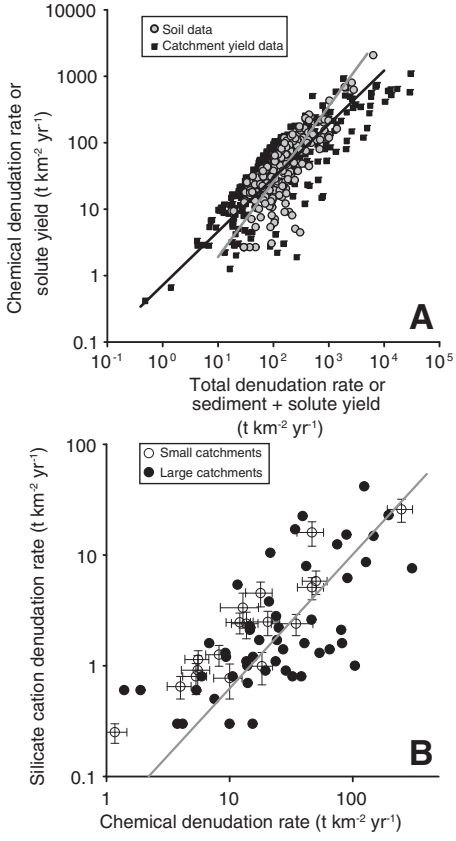

Figure 1. A: Soil chemical denudation rate versus total denudation rate and catchment solute yield versus the sum of solute and sediment yields. Reduced major axis (RMA) regression relationship fit to the soils data is: $y = 0.14(+0.04/-0.03)x^{1.13(\pm0.05)}$; R^2 = 0.62 and the fit to the catchment yield data is: $y = 0.71(+0.12/-0.10)x^{0.81(\pm0.03)}$; R^2 = 0.64. Soil values are based on 188 ^{10}Be and chemical depletion values compiled by Larsen et al. (2014); see the Data Repository (see footnote 1) for sources. The catchment yield relationship is used to model chemical denudation rates and is based on data for 299 rivers compiled by Milliman and Farnsworth (2011). Chemical denudation rates predicted by catchment data model use a retransformation bias correction factor of 1.4, determined following Dingman (2009). B: Silicate cation denudation rate versus chemical denudation rate data from large (Gaillardet et al., 1999) and small (West et al., 2005) catchments. The RMA regression relationship fit to the combined data sets is: $y = 0.09(+0.03/-0.02)x^{1.03(\pm0.09)}$; R^2 = 0.51. Values for small catchments are means of several catchments within a region (West et al., 2005) (± indicates 1 standard error).

*Current address: Division of Geological and Planetary Sciences, California Institute of Technology, Pasadena, California 91125, USA.

anthropogenic acceleration of erosion (Milliman and Syvitski, 1992). Global solute yields are thought be ~3.8 Gt yr^{-1}, such that the annual yield of sediment and solutes to the oceans is ~23 Gt (Milliman and Farnsworth, 2011).

Catchment-scale denudation rate (^{10}Be) and sediment yield data are both spatially limited, but calibrated relationships between measured values and independent predictor variables can be used in a spatial modeling framework to predict and estimate global-scale sediment yields or denudation rates (e.g., Pelletier, 2012; Cohen et al., 2013; Willenbring et al., 2013). We modeled global-scale denudation as a function of slope, exploiting the finding that mean catchment slope is the dominant predictor of denudation rates (Portenga and Bierman, 2011), and modeled chemical denudation rates as a function of total denudation rates. We then compared the modeled denudation rates to reported sediment and solute yields (Milliman and Farnsworth, 2011) to estimate the contribution of mountains to global denudation, and explore potential implications for the global carbon cycle.

METHODS

Slope data used for global-scale denudation modeling were based on a 3 arc-second (~90 m pixels at the equator) digital elevation model (DEM) with worldwide coverage, obtained from www.viewfinderpanoramas.org. The DEM consists of Shuttle Radar Topography Mission (SRTM) elevation data with coverage gaps and high-latitude areas filled with digitized topographic map data of varying scales. Slope angles were calculated by accounting for the latitudinal dependence on grid cell shape caused by the poleward convergence of meridians. We also determined mean local slope by centering a 5 × 5 km square on each grid cell and then calculating the mean slope of all grid cells within the square. Slope and mean local slope angle distributions were extracted from the DEM, as well as versions of the DEM generated by removing lakes with areas >50 km^2 (World Wildlife Fund GLWD-1 data; worldwildlife.org/pages/global-lakes-and-wetlands-database) and by removing both lakes and closed (endorheic) basins (United Nations Food and Agriculture Organization watershed data; fao.org/geonetwork/srv/en/metadata.show?id=38047). Due to extensive ice cover, we excluded Antarctica and Greenland from our analyses.

Denudation rates (D, mm yr^{-1}), were modeled using the mean local slope (tangent θ) grid as: $D = 0.0119\ (+0.00091/–0.00085)\ e^{6.5(\pm0.21)\cdot\tan\theta}$ (±1 standard error). This nonlinear relationship was derived by Willenbring et al. (2013) based on a compilation of 990 in situ ^{10}Be-based watershed-scale denudation measurements and mean catchment slope values derived from 3 arc-second SRTM DEM data. Uncertainty in D was assessed by using the upper and lower 68th percentile prediction intervals on the above equation to model upper and lower bounds on denudation rates for each pixel. Our approach diverges from that of Willenbring et al. (2013) in that they used this relationship to model global denudation using a 30 arc-second DEM, whereas we use a 3 arc-second DEM that matches the resolution of the DEM used to calibrate the denudation rate-slope relationship to avoid issues associated with the scale dependence of slope and DEM grid scale (Zhang and Montgomery, 1994).

To assess the effect of grid size on our analysis, we calculated slopes from DEMs with grid sizes from 2 m to 1 km for four upland study areas with lidar data: in the Cascade Mountains, Oregon Coast Range, California Coast Range, and San Gabriel Mountains of the western United States. We used the slope data to calibrate a scaling relationship between mean slope and DEM grid scale. For comparison, slope and denudation rate distributions were also determined using a 30 arc-second DEM that was generated by resampling the 3 arc-second data.

The catchment denudation-slope relationship predicts unrealistically high denudation rates (i.e., >10 m yr^{-1}) for very steep mean local slope values (i.e., >45°) that reflect what we interpret to be artifacts that affect <0.001% of the DEM. Therefore, to avoid overprediction of denudation rates we imposed a maximum denudation rate of 10 mm yr^{-1}, a value close to the most rapid denudation rates that have been measured using ^{10}Be (Larsen et al., 2014). Chemical denudation rates were calculated as a function of D using an empirical relationship derived from a compilation of catchment sediment and solute yield data (Fig. 1A).

We tallied the results for individual grid cells to generate cumulative distributions of slope and mean local slope, a cumulative distribution of denudation rates as a function of slope angle, and estimates of annual global denudation. The cumulative distributions were normalized to the area of Earth's terrestrial surface and account for latitudinal variation in grid cell area. Annual global denudation estimates employ a correction factor of 2.2 that accounts for retransformation bias that occurs when predicting denudation rates using the equation herein (Miller, 1984; Willenbring et al., 2014). Predicted catchment denudation rates were compared against measurements from 265 catchments with both sediment and solute flux data (Milliman and Farnsworth, 2011), and we assessed how the ratio of measured yields to catchment denudation rates varied as a function of catchment area.

RESULTS

The lidar data show that, for each of the four sites, mean slope angles decline as DEM grid scale coarsens (Fig. 2A). The ratio of the mean slope for a given DEM scale to the mean slope from the 2 m DEM declines logarithmically as DEM scale increases (Fig. 2B). The magnitude of this effect increases as the topography steepens, with a uniformly pronounced decline in mean slope between 90 m and 1 km grid sizes, indicating that coarse-scale DEMs greatly and systematically underrepresent the relative proportion of steep slopes. For example, the mean slope angle at the site with the lowest slope angles (California Coast Range) is 21° for the 2 m DEM, 14° for the 90 m DEM, and just 2° for the 1 km DEM. Whereas at the steeper Oregon Coast Range site, the mean slope angle is 30° for the 2 m DEM, 17° for the 90 m DEM, and just 3° for the 1 km DEM.

The global 3 arc-second DEM data indicate that ~9% of Earth's surface has mean local slopes steeper than 15°, which corresponds to slopes >24° at 2 m grid scale, based on the relationship in Figure 2B, and in map view tracks

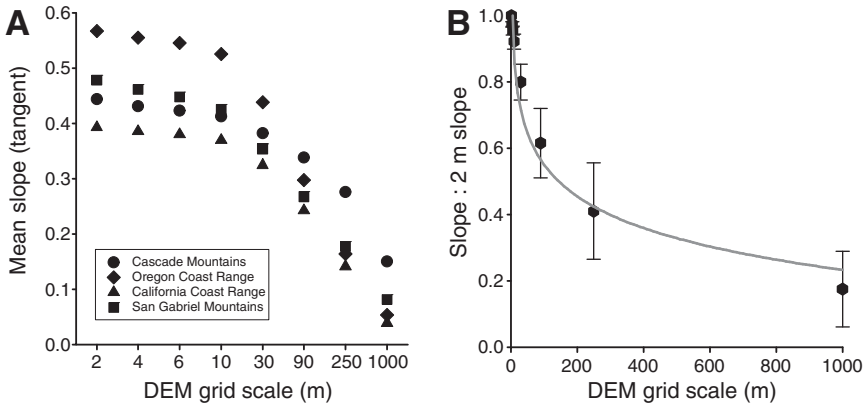

Figure 2. A: Mean slope declines as a function of digital elevation model (DEM) grid scale at four sites with lidar topographic data; the Cascade Mountains (12122 km^2), Oregon Coast Range (418 km^2), California Coast Range (11 km^2), and San Gabriel Mountains (57 km^2) in the western United States (see the Data Repository [see footnote 1] for locations). B: Ratio of mean slope for DEM with given scale to mean slope from 2 m DEMs of the four study areas. Symbols show mean slope averaged across the four sites and the standard deviation. Mean slope declines logarithmically with increasing DEM grid scale as: $y = –0.14\ln(x) + 1.19$; $R^2 = 0.96$.

Earth's mountain ranges (Fig. 3A; Fig. DR1 in the GSA Data Repository[1]). Removing lakes and closed basins from the analysis shifts the mean local slope distribution only slightly, such that this value changes to ~10% of Earth's surface topography (Fig. DR2).

Modeling at 3 arc-second scale shows that areas with steep slopes, though small in terms of Earth's terrestrial surface area, contribute disproportionately to denudation; areas with mean local slopes >15° contribute 52% of the global denudation (Fig. 3B). Global denudation is estimated to be 28 (+64/–20) Gt yr^{-1} (assuming a rock density of 2650 kg m^{-3}); by subtracting denudation that occurs in closed basins, we estimate that 23 (+53/–16) Gt of material is made available for delivery to oceans each year. Approximately 40% of global chemical denudation is predicted to occur on areas with local mean slopes >15° and, given that the relationship between silicate and total chemical denudation is approximately linear (Fig. 1B), a similar proportion of global silicate denudation likely occurs in mountains. Chemical denudation on the ocean-draining land area is estimated to be 3.9 (+6.2/–2.4; including uncertainty in *D* only) Gt yr^{-1}.

Globally, modeled catchment denudation rates are correlated (R^2 = 0.44, $p < 0.0001$) with the sum of river sediment and solute yields (Fig. 4A). However, the ratio between them varies an order of magnitude either way; in many basins, predicted catchment denudation exceeds sediment yields by as much as an order of magnitude. In many others, the relationship is reversed, with sediment yields exceeding catchment denudation by up to an order of magnitude. A wide range of factors influence the relationship between denudation and sediment yields through changes in sediment storage, such as is reflected in the decline in the ratio of river yield to catchment denudation with increasing drainage area (Fig. 4B). The wide range of values in this ratio reflects additional factors, including how dams and land use can greatly decrease or increase modern sediment yields relative to long-term catchment denudation, as well as the inherent uncertainty and errors in both our model predictions and measured yield estimates.

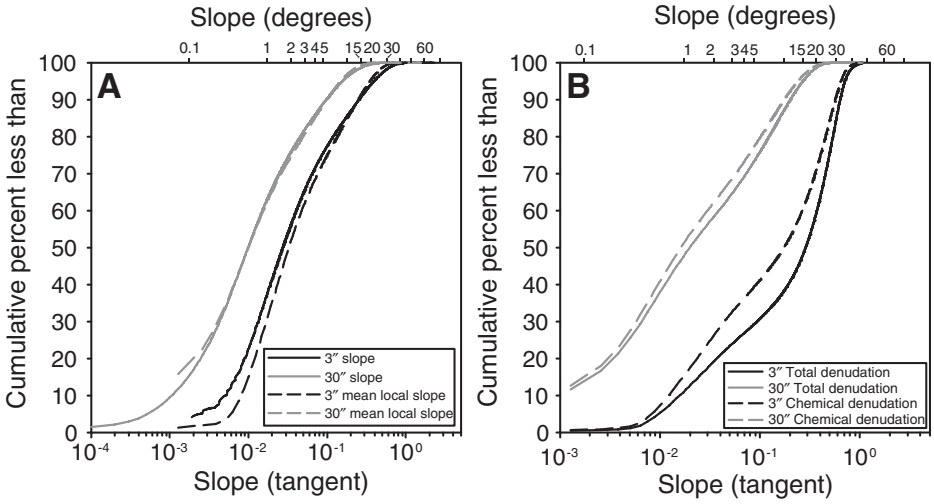

Figure 3. A: Cumulative distributions of global slope and mean local slope (slope averaged with a 5 × 5 km moving window) for both 3 arc-second (″) and 30 arc-second digital elevation models (DEMs). B: Cumulative distributions of global denudation (total) and chemical denudation as function of slope for 3 arc-second and 30 arc-second DEMs.

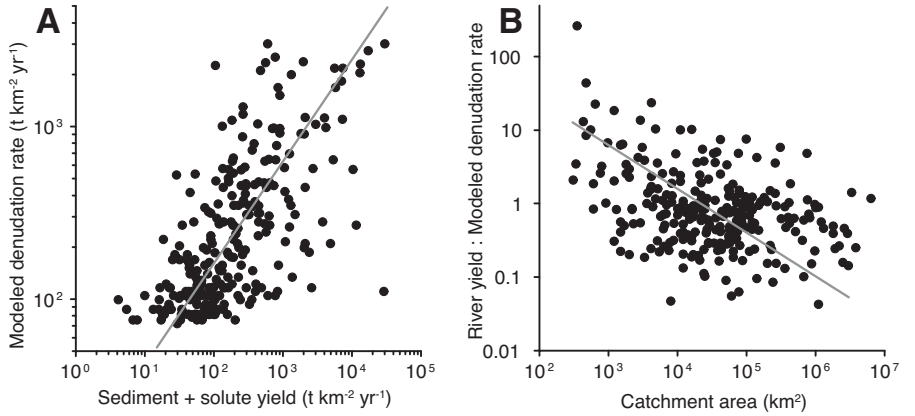

Figure 4. A: Modeled denudation rates increase with the sum of sediment and solute yields for 265 catchments [$y = 10.6(+0.10/–0.10)x^{0.59(\pm0.03)}$; $R^2 = 0.44$]. B: Ratio of modeled denudation to the sum of sediment and solute yields declines as function of catchment area [$y = 383(+22/–21)x^{-0.60(\pm0.03)}$; $R^2 = 0.15$; ± indicates 1 standard error].

DISCUSSION

The strong grid-scale dependence of slope apparent in our analysis is consistent with previous results from analyses of much smaller areas of the Oregon Coast Range (Mettman Ridge, 0.3 km^2) and California Coast Range (Tennessee Valley, 1.2 km^2) sites (Zhang and Montgomery, 1994). Our results suggest that 10 m DEMs reasonably represent slopes, that slopes are underestimated by several degrees as grid scale increases to 30 and 90 m scales. Coarser-scale DEMs poorly represent steep topography; at 30 arc-second resolution, <1% of mean local slopes exceed 15° globally. Denudation rates increase non-linearly with increasing slope—as calibrated with 3 arc-second data (Willenbring et al., 2013). Hence the lack of steep topography at 30 arc-second resolution explains why the modeled contribution of steep slopes to global denudation and the magnitude of the global denudation rate estimated by us (10.1 Gt for the ocean-draining land area) and by Willenbring et al. (2013) using 30 arc-second data are both much lower than our estimates that use 3 arc-second slope data.

Our denudation model results are consistent with a compilation of worldwide river load data that indicate that steep, wet mountains contribute 62% of sediment, 38% of dissolved solids, and 60% of dissolved silicate to Earth's oceans, although such topography makes up only 14% of the ocean-draining land surface (Milliman and Farnsworth, 2011). The modeled global denudation rate is comparable to the sum of the global sediment and solute yields of ~23 Gt yr^{-1} (Milliman and Farnsworth (2011). The estimated physical denudation of the ocean-draining land surface of 19 Gt yr^{-1} (calculated by subtracting the chemical denudation from the total denudation) is equal to the most recent global sediment yield estimate of 19 Gt yr^{-1}, and our chemical denudation estimate of 3.9 Gt yr^{-1} is close to the global solute yield estimate of 3.8 Gt yr^{-1} (Milliman and Farnsworth, 2011). However, we emphasize that there is no *a priori* reason that denudation rates and river yields should balance (Covault et al., 2013; Warrick et al., 2014). The

[1]GSA Data Repository item 2014186, description of data sources, Figures DR1 (global slope maps), DR2 (global slope angle distributions), DR3 (lidar site map), and DR4 (lidar slope angle distributions), is available online at www.geosociety.org/pubs/ft2014.htm, or on request from editing@geosociety.org or Documents Secretary, GSA, P.O. Box 9140, Boulder, CO 80301, USA.

denudation rate-slope relationship both exhibits less nonlinearity than relationships from individual landscapes (e.g., DiBiase et al., 2010) and underestimates the highest measured denudation rates, and hence underpredicts global denudation. Humans have caused sediment yields to increase—by as much as a factor of two (Milliman and Syvitski, 1992), deposition of sediment in floodplains and basins stores sediment upstream from oceans (e.g., Walling, 1983), and sediment gauging records may capture few high-magnitude, low-frequency events (Kirchner et al., 2001; Covault et al., 2013); these factors are among many others that cause divergence in denudation rates and sediment yields.

The modeling results indicate that denudation is apportioned approximately equally between the ~10% of the world's land surface with slopes >15° (or a "true" slope of 24°, estimated using the relationship in Fig. 2B) and the 90% of more gently sloping topography. The magnitude of global denudation is therefore sensitive to the proportion of Earth's surface with mountainous topography. For example, given our predicted annual global denudation rate of 23 Gt yr^{-1}, replacing 1% of Earth's gently sloping surface (<15°) with steep slopes (>15°) would disproportionately increase global denudation rates by nearly 5%, and chemical denudation rates by more than 3%. Although our results do not address CO_2 sources from mountains (e.g., Bickle, 1996; Torres et al., 2014), the high proportion of global denudation attributable to mountains and the positive links among total denudation, chemical denudation, and silicate cation denudation rates are consistent with the view that mountains are an important link in the geological carbon cycle.

CONCLUSIONS

Modeling global denudation with a 3 arc-second DEM demonstrates that mountains dominate global denudation. Given that chemical weathering rates increase with total denudation rates, silicate weathering and the associated CO_2 drawdown are expected to be closely linked to the area of Earth's surface with steep topography. Therefore, understanding Earth's physiographic history, and its influence on physical and chemical denudation rates, is essential for understanding the geological carbon cycle.

ACKNOWLEDGMENTS

We thank the Puget Sound Lidar Consortium, the Oregon Department of Geology and Mineral Industries, the National Center for Airborne Laser Mapping, the National Science Foundation OpenTopography Facility, and viewfinderpanoramas.org for providing topographic data. We also thank Josh West for insightful discussion and Alex Densmore, Kelin Whipple, and an anonymous reviewer for comments that greatly improved the manuscript. Larsen's work on this project was supported by NASA Earth and Space Science Fellowship NNX09AN90H and the California Institute of Technology Division of Geological and Planetary Sciences.

REFERENCES CITED

Berner, R.A., 1991, A model for atmospheric CO_2 over Phanerozoic time: American Journal of Science, v. 291, p. 339–376, doi:10.2475/ajs.291.4.339.

Berner, R.A., and Caldeira, K., 1997, The need for mass balance and feedback in the geochemical carbon cycle: Geology, v. 25, p. 955–956, doi:10.1130/0091-7613(1997)025<0955:TNFMBA>2.3.CO;2.

Bickle, M.J., 1996, Metamorphic decarbonation, silicate weathering and the long-term carbon cycle: Terra Nova, v. 8, p. 270–276, doi:10.1111/j.1365-3121.1996.tb00756.x.

Bierman, P., and Steig, E.J., 1996, Estimating rates of denudation using cosmogenic isotope abundances in sediment: Earth Surface Processes and Landforms, v. 21, p. 125–139, doi:10.1002/(SICI)1096-9837(199602)21:2<125::AID-ESP511>3.0.CO;2-8.

Chamberlin, T.C., 1899, An attempt to frame a working hypothesis of the cause of glacial periods on an atmospheric basis: Journal of Geology, v. 7, p. 545–584, doi:10.1086/608449.

Cohen, S., Kettner, A.J., Syvitski, J.P.M., and Fekete, B.M., 2013, WBMsed, a distributed global-scale riverine sediment flux model: Model description and validation: Computers & Geosciences, v. 53, p. 80–93, doi:10.1016/j.cageo.2011.08.011.

Covault, J.A., Craddock, W.H., Romans, B.W., Fildani, A., and Gosai, M., 2013, Spatial and temporal variations in landscape evolution: Historic and longer-term sediment flux through global catchments: Journal of Geology, v. 121, p. 35–56, doi:10.1086/668680.

DiBiase, R.A., Whipple, K.X., Heimsath, A.M., and Ouimet, W.B., 2010, Landscape form and millennial erosion rates in the San Gabriel Mountains, CA: Earth and Planetary Science Letters, v. 289, p. 134–144, doi:10.1016/j.epsl.2009.10.036.

Dingman, S.L., 2009, Fluvial hydraulics: Oxford, UK, Oxford University Press, 559 p.

France-Lanord, C., and Derry, L.A., 1997, Organic carbon burial forcing of the carbon cycle from Himalayan erosion: Nature, v. 390, p. 65–67, doi:10.1038/36324.

Gaillardet, J., Dupré, B., Louvat, P., and Allégre, C.J., 1999, Global silicate weathering and CO_2 consumption rates deducted from the chemistry of large rivers: Chemical Geology, v. 159, p. 3–30, doi:10.1016/S0009-2541(99)00031-5.

Hilton, R.G., Galy, A., Hovius, N., Kao, S.-J., Horng, S.-J., and Chen, H., 2012, Climatic and geomorphic controls on the erosion of terrestrial biomass from subtropical mountain forest: Global Biogeochemical Cycles, v. 26, p. 1–12, GB3014, doi:10.1029/2012GB004314.

Kirchner, J.W., Finkel, R.C., Riebe, C.S., Granger, D.E., Clayton, J.L., King, J.G., and Megahan, W.F., 2001, Mountain erosion over 10 yr, 10 k.y., and 10 m.y. time scales: Geology, v. 29, p. 591–594, doi:10.1130/0091-7613(2001)029<0591:MEOYKY>2.0.CO;2.

Larsen, I.J., Almond, P.C., Eger, A., Stone, J.O., Montgomery, D.R., and Malcolm, B., 2014, Rapid soil production and weathering in the Southern Alps, New Zealand: Science, v. 343, p. 637–640, doi:10.1126/science.1244908.

Miller, D.M., 1984, Reducing transformation bias in curve fitting: American Statistician, v. 38, p. 124–126.

Milliman, J., and Farnsworth, K., 2011, River discharge to the coastal ocean: A global synthesis: New York, Cambridge University Press, 384 p.

Milliman, J.D., and Syvitski, J.P., 1992, Geomorphic/tectonic control of sediment discharge to the ocean: The importance of small mountainous rivers: Journal of Geology, v. 100, p. 525–544, doi:10.1086/629606.

Molnar, P., and England, P., 1990, Late Cenozoic uplift of mountain ranges and global climate change: Chicken or egg?: Nature, v. 346, p. 29–34, doi:10.1038/346029a0.

Montgomery, D., and Brandon, M., 2002, Topographic controls on erosion rates in tectonically active mountain ranges: Earth and Planetary Science Letters, v. 201, p. 481–489, doi:10.1016/S0012-821X(02)00725-2.

Pelletier, J.D., 2012, A spatially distributed model for the long-term suspended sediment discharge and delivery ratio of drainage basins: Journal of Geophysical Research, v. 117, F02028, doi:10.1029/2011JF002129.

Portenga, E.W., and Bierman, P.R., 2011, Understanding Earth's eroding surface with ^{10}Be: GSA Today, v. 21, p. 4–10, doi:10.1130/G111A.1.

Raymo, M., and Ruddiman, W., 1992, Tectonic forcing of late Cenozoic climate: Nature, v. 359, p. 117–122, doi:10.1038/359117a0.

Raymo, M., Ruddiman, W., and Froelich, P., 1988, Influence of late Cenozoic mountain building on ocean geochemical cycles: Geology, v. 16, p. 649–653, doi:10.1130/0091-7613(1988)016<0649:IOLCMB>2.3.CO;2.

Summerfield, M., and Hulton, N., 1994, Natural controls of fluvial denudation rates in major world drainage basins: Journal of Geophysical Research, v. 99, p. 13,871–13,883, doi:10.1029/94JB00715.

Syvitski, J.P., Vörösmarty, C.J., Kettner, A.J., and Green, P., 2005, Impact of humans on the flux of terrestrial sediment to the global coastal ocean: Science, v. 308, p. 376–380, doi:10.1126/science.1109454.

Torres, M.A., West, A.J., and Li, G., 2014, Sulphide oxidation and carbonate dissolution as a source of CO_2 over geological timescales: Nature, v. 507, p. 346–349, doi:10.1038/nature13030.

von Blanckenburg, F., 2005, The control mechanisms of erosion and weathering at basin scale from cosmogenic nuclides in river sediment: Earth and Planetary Science Letters, v. 237, p. 462–479, doi:10.1016/j.epsl.2005.06.030.

Walling, D.E., 1983, The sediment delivery problem: Journal of Hydrology, v. 65, p. 209–237, doi:10.1016/0022-1694(83)90217-2.

Warrick, J.A., Milliman, J.D., Walling, D.E., Wasson, R.J., Syvitski, J.P.M., and Aalto, R.E., 2014, Earth is (mostly) flat: Apportionment of the flux of continental sediment over millennial time scales: Comment: Geology, v. 42, p. e316, doi:10.1130/G34846C.1.

West, A.J., Galy, A., and Bickle, M., 2005, Tectonic and climatic controls on silicate weathering: Earth and Planetary Science Letters, v. 235, p. 211–228, doi:10.1016/j.epsl.2005.03.020.

Willenbring, J.K., and von Blanckenburg, F., 2010, Long-term stability of global erosion rates and weathering during late-Cenozoic cooling: Nature, v. 465, p. 211–214, doi:10.1038/nature09044.

Willenbring, J., Codilean, A., and McElroy, B., 2013, Earth is (mostly) flat: Apportionment of the flux of continental sediment over millennial time scales: Geology, v. 41, p. 343–346, doi:10.1130/G33918.1.

Willenbring, J., Codilean, A., and McElroy, B., 2014, Earth is (mostly) flat: Apportionment of the flux of continental sediment over millennial time scales: Reply: Geology, v. 42, p. e317, doi:10.1130/G35326Y.1.

Zhang, W., and Montgomery, D.R., 1994, Digital elevation model grid size, landscape representation, and hydrologic simulations: Water Resources Research, v. 30, p. 1019–1028, doi:10.1029/93WR03553.

Manuscript received 20 September 2013
Revised manuscript received 23 March 2014
Manuscript accepted 25 March 2014

Printed in USA